Establishment of the early cilia preassembly protein complex during motile ciliogenesis

Amjad Horani[a,1], Alessandro Ustione[b], Tao Huang[c], Amy L. Firth[d], Jiehong Pan[c], Sean P. Gunsten[c], Jeffrey A. Haspel[c], David W. Piston[b], and Steven L. Brody[c]

[a]Department of Pediatrics, Washington University School of Medicine, St. Louis, MO 63110; [b]Department of Cell Biology and Physiology, Washington University School of Medicine, St. Louis, MO 63110; [c]Department of Medicine, Washington University School of Medicine, St. Louis, MO 63110; and [d]Department of Medicine, University of Southern California, Keck School of Medicine, Los Angeles, CA 90033

Edited by Kathryn V. Anderson, Sloan Kettering Institute, New York, NY, and approved December 27, 2017 (received for review September 9, 2017)

Motile cilia are characterized by dynein motor units, which preassemble in the cytoplasm before trafficking into the cilia. Proteins required for dynein preassembly were discovered by finding human mutations that result in absent ciliary motors, but little is known about their expression, function, or interactions. By monitoring ciliogenesis in primary airway epithelial cells and MCIDAS-regulated induced pluripotent stem cells, we uncovered two phases of expression of preassembly proteins. An early phase, composed of HEATR2, SPAG1, and DNAAF2, preceded other preassembly proteins and was independent of MCIDAS regulation. The early preassembly proteins colocalized within perinuclear foci that also contained dynein arm proteins. These proteins also interacted based on immunoprecipitation and Förster resonance energy transfer (FRET) studies. FRET analysis of HEAT domain deletions and human mutations showed that HEATR2 interacted with itself and SPAG1 at multiple HEAT domains, while DNAAF2 interacted with SPAG1. Human mutations in HEATR2 did not affect this interaction, but triggered the formation of p62/Sequestosome-1–positive aggregates containing the early preassembly proteins, suggesting that degradation of an early preassembly complex is responsible for disease and pointing to key regions required for HEATR2 scaffold stability. We speculate that HEATR2 is an early scaffold for the initiation of dynein complex assembly in motile cilia.

ciliopathy | cilia | genetics | preassembly | primary ciliary dyskinesia

Cilia project into the extracellular environment for sensory function or motility. Motile cilia are distinguished from sensory primary cilia by the presence of motor proteins that are required to move fluid in the brain, respiratory, and reproductive tracts. Large multiprotein motor complexes known as the outer dynein arms (ODAs) and inner dynein arms (IDAs) localize on each of nine doublets of microtubules of the axoneme. The dynein arms include AAA-ATPase family dynein proteins required for ATP hydrolysis to power ciliary motility. The ODA is composed of at least 16 proteins that form an almost 2-MDa complex for axoneme sliding (1), while the IDA contains no less than 12 subunits also functioning in sliding and the regulation of aspects of ciliary motion (2–4).

Human mutations that result in the loss of the ODA on electron micrographs were first identified in dynein motor genes *DNAH5* and *DNAI1* using a candidate approach based on conserved structures in the flagellated alga *Chlamydomonas rheinhardtii* (5, 6). Owing to the complexity of motile cilia (7), mutations in nearly 40 genes are now known to cause primary ciliary dyskinesia (PCD) and result in sinopulmonary infection, bronchiectasis, otitis media, laterality, and cardiac defects (8, 9). Mutations that result in an absence of both the ODA and IDA were more recently discovered. The proteins coding from these genes are not detected in the cilia but, instead, are present only in the cytoplasm, and include DNAAF1 (LRRC50, ODA7) (10), DNAAF2 (KTU, PF13) (11), LRRC6 (12, 13), HEATR2 (DNAAF5) (14), DNAAF3 (PF22) (15), DYX1C1 (16), SPAG1 (17), ZMYND10 (18), C21orf59 (Kurly, FBB18) (19), and PIH1D3 (20, 21). The function of these proteins is unknown; however, missing dynein motor complexes in the cilia of mutants and cytoplasmic localization (or absence in the cilia proteome) suggest a role in the preassembly of dynein motor complexes. Studies in *C. reinhardtii* show motor components in the cell body before transport to flagella (22–25). However, the expression, interactions, and functions of preassembly proteins, as well as the steps required for preassembly, are undefined.

We have previously reported that mutations in the gene coding for the cytoplasmic protein HEATR2 result in absence of the ODA and IDA, and point to a role in dynein arm preassembly through an undetermined mechanism (14). HEATR2 is a HEAT-repeat protein containing at least 10 HEAT motif domains that span the protein. HEAT domains are tandem sequences of 37–47 amino acids that form two α-helical structures linked by a short loop. Structural analysis of HEAT-repeat proteins shows that the HEAT domains are stacked together to form characteristic concave structures (26–28). Owing to twists of the α-helixes, HEAT-repeat proteins exhibit flexibility that favor the formation of scaffolds for large complexes (26, 29). Among the best characterized is the A subunit (PPP2R1), which supports the heterotrimeric protein phosphatase 2A (PP2A) (27).

Ciliogenesis requires the rapid production of thousands of axonemal dynein motor complexes that will be docked at 24- to 96-nm intervals along the 5- to 10-μm length of each of 200–300 cilia per cell (30). We previously observed that HEATR2 is

Significance

Motile cilia preassembly proteins processing dynein motor proteins have been identified in patients with motile cilia dysfunction. However, the exact function and interaction of these proteins are not understood. Using primary airway cell culture and regulated induced pluripotent stem cell culture, we provide a roadmap for preassembly protein expression, showing that HEATR2 is the first preassembly protein to appear, emerging early in ciliogenesis and preceding known regulatory factors. HEATR2, SPAG1, and DNAAF2 colocalize within previously unrecognized cytoplasmic foci to form an early preassembly complex. The findings suggest that a lead scaffold structure essential for motile cilia function is destroyed by proteostasis in HEATR2 mutants, leading to degradation of the whole preassembly complex and identifying the cellular mechanism for disease.

Author contributions: A.H., D.W.P., and S.L.B. designed research; A.H., A.U., T.H., A.L.F., J.P., S.P.G., and J.A.H. performed research; A.H., A.U., A.L.F., and J.A.H. contributed new reagents/analytic tools; A.H., A.U., T.H., A.L.F., J.P., S.P.G., J.A.H., D.W.P., and S.L.B. analyzed data; and A.H. and S.L.B. wrote the paper.

The authors declare no conflict of interest.

This article is a PNAS Direct Submission.

[1]To whom correspondence should be addressed. Email: horani_a@wustl.edu.

This article contains supporting information online at www.pnas.org/lookup/suppl/doi:10.1073/pnas.1715915115/-/DCSupplemental.

present diffusely within the cytoplasm, suggesting that preassembly proteins are active at multiple sites (14). Here, our analysis of the temporal expression of known preassembly proteins during ciliogenesis identified HEATR2 as the earliest expressed. We uncovered a biphasic pattern of preassembly protein expression, with an early phase composed of HEATR2, SPAG1, and DNAAF2, which form an initial complex within cytoplasmic preassembly foci to support the proper assembly of the IDA and ODA.

Results

Cilia Preassembly Follows a Biphasic Expression Pattern. To begin to understand the preassembly pathway, we examined the relative expression of the known human preassembly proteins (10, 11, 13, 15–18, 21), as temporal relationships are not reported. We used in vitro differentiation of normal human tracheobronchial epithelial cells (hTECs) cultured at the air–liquid interface (ALI) to induce multiciliogenesis, which generates cilia by ALI day 14 (31, 32) (Fig. S1*A*). Expression of mRNA was assayed during differentiation and compared with ciliogenesis transcription factors *MCIDAS* and *FOXJ1*. Transcripts of preassembly genes *HEATR2*, *SPAG1* (long form), and *DNAAF2* were expressed during the early stages of airway epithelial cell differentiation, preceding the expression of *FOXJ1* (ALI day 7), which directs the transcription of most cilia components (33, 34), Levels of these three genes were different from other preassembly genes as determined by K-means cluster analysis (Fig. 1*A*, Fig. S1*B*, and Table S1). A second phase of preassembly genes composed of *DNAAF1*, *DNAAF3*, *DYX1C1*, *LRRC6*, *ZMYND10*, and *PIH1D3* was expressed after ALI day 7, coincident with the onset of *FOXJ1* (Fig. S1*B* and Table S1).

MCIDAS is required for centriolar replication and activation of *FOXJ1* for the regulation of motile cilia-specific proteins (35). To determine if the early expression of *HEATR2*, *SPAG1*, and *DNAAF2* follows canonical *MCIDAS-FOXJ1* regulation, we used an induced pluripotent stem cell (iPSC) culture system to conditionally express *MCIDAS* in all cells differentiated to the lung epithelial fate (36). In the presence of doxycycline activation, *MCIDAS* did not induce *HEATR2* or *DNAAF2*, and minimally increased *SPAG1* expression (Fig. 1*B* and Fig. S2*A*). By comparison, other preassembly factors were expressed at a later stage of differentiation and responded to regulation by MCIDAS (Figs. S1*B* and S2*A*). The early expression of *HEATR2*, *SPAG1*, and *DNAAF2* is contrary to the current paradigm that places cilia preassembly downstream to FOXJ1 (35), and is further evidenced by detection of HEATR2, SPAG1, and DNAAF2 in the trachea epithelial cells of Foxj1$^{-/-}$ mice (37) (Fig. S2*B*).

HEATR2, SPAG1, and DNAAF2 Are Coexpressed Early, Within Distinct Puncta. At the protein levels, HEATR2, SPAG1, and DNAAF2 showed early onset during differentiation, in relation to FOXJ1 (Fig. 1*C*). HEATR2 levels were prominent early in differentiation, and were accompanied by at least two dominant bands of SPAG1 (at ~100 kDa), as previously noted (17, 38) (Fig. 1*C* and Fig. S3). Our immunoblot analysis of SPAG1 also showed multiple short fragments, as reported by others (17, 38). These fragments were detected by SPAG1 antibodies that target either the amino (N) or carboxy (C) terminus (Fig. S3*A*). As previously suggested, these fragments are likely nonspecific (17, 38).

At ALI day 0, HEATR2 was intranuclear, and by ALI day 3, it was localized to puncta within the cytoplasm of hTECs (Fig. 1*D*). The pattern of expression within puncta persisted as airway cells differentiated into mature multiciliated cells, cultured at ALI for 21 d or more (14). The onset of SPAG1 and DNAAF2, as detected by immunostaining, was slightly later, present by ALI day 3. However, the intracellular protein localization was similar to HEATR2, and both were present as puncta within the cytoplasm (Fig. 1 *C* and *D*). The early preassembly proteins were present in cells before the appearance of dynein DNAI1, a FOXJ1-dependent member of the ODA (39) (Fig. 1*C*). During active cilia growth, DNAI1 colocalized with HEATR2 in the cytoplasm (ALI day 13), positioning a known ODA subunit with an early preassembly protein (Fig. 1*E*). HEATR2 expression also precedes the massive

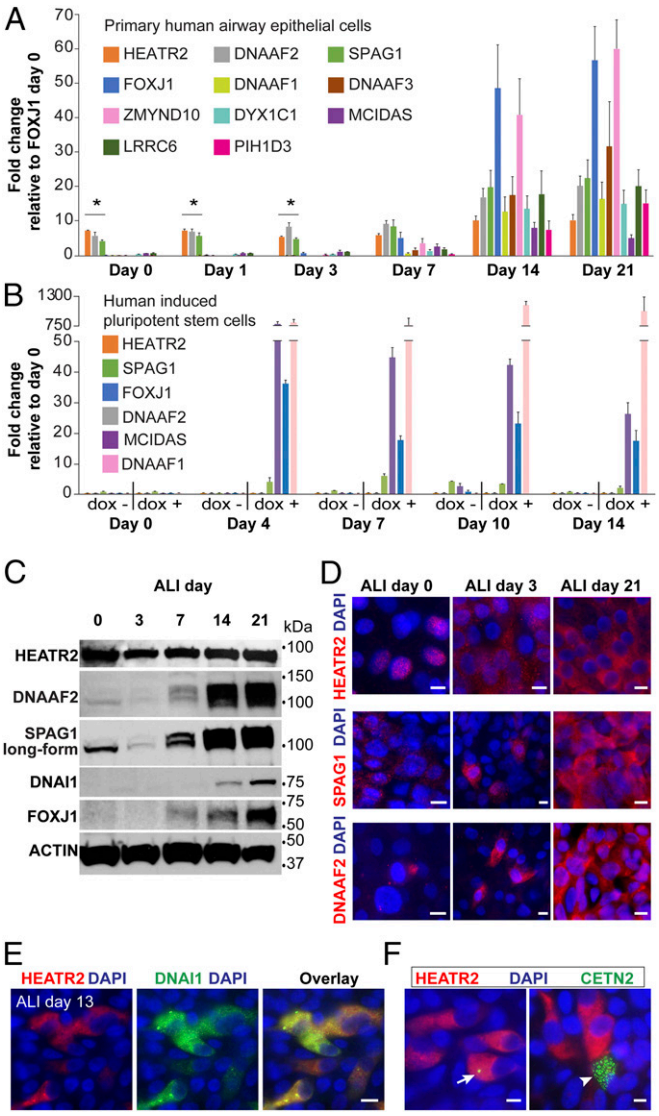

Fig. 1. Biphasic expression of cilia preassembly gene during differentiation. (*A*) mRNA levels of cilia preassembly genes and transcription factors *MCIDAS* and *FOXJ1* detected by RT-PCR. The hTECs were cultured at the ALI, and mRNA was measured at the indicated day. Levels are shown relative to each gene, normalized to *FOXJ1* expression at ALI day 0. (*B*) Cilia preassembly gene mRNA levels following induced *MCIDAS* expression during ALI culture. Lung epithelial cells were derived from iPSCs that expressed *MCIDAS* controlled by a tetracycline-regulated element for treatment with (dox+) or without (dox–) doxycycline initiated at ALI day 0. Data are normalized to *Actin*, and expressed as the fold change relative to ALI day 0. (*C*) Immunoblot analysis of early preassembly factors compared with FOXJ1 and DNAI1. (*D*) HEATR2, SPAG1, and DNAAF2 in hTECs at indicated day ALI. (*E*) HEATR2 (red) and DNAI1 (green) at ALI day 13, detected by immunofluorescence. (*F*) HEATR2 (red) relative to centriolar replication marked by CETN2 (green) in hTECs at ALI day 13. HEATR2 presents in cells before centriolar replication. The arrow points to a centrosome, and the arrowhead points to amplified centrioles. Nuclei were stained with DAPI (blue). (Scale bars: *D–F*, 10 μM.) *A* and *B* are the mean ± SEM of three independent preparations. In *A*, the expression of the indicated preassembly genes (*) is partitioned from other genes by K-means cluster analysis (sample size: 44–64 data points per day ALI).

centriole replication required to form the basal bodies for cilia nucleation (Fig. 1*F*), which had been previously identified as one of the earliest markers of motile ciliogenesis (31, 40). Together, these data suggest that motile cilia preassembly occurs in sequential stages, with a set of early preassembly factors preceding *FOXJ1* and independent of *MCIDAS* and a late phase composed of additional *MCIDAS*/*FOXJ1*-dependent proteins.

HEATR2 Interacts with Early Preassembly Proteins DNAAF2 and SPAG1. Similarities in the expression patterns between HEATR2, SPAG1, and DNAAF2 suggested that these proteins might interact as an early preassembly complex. Immunostaining of mature multiciliated cells in normal human trachea shows a shared characteristic pattern (Fig. 2*A*). Foci with bright staining were typically observed within the perinuclear region (Fig. 2*A*, *Inset*), while smaller puncta were present diffusely in the cytoplasm, as early as ALI day 3 (Fig. 1*D*), and in the mature airway (Fig. 2*A*). Same-species primary antibodies for the three early preassembly proteins limited the ability to identify relationships; however, staining with fluorescently labeled Fab fragments bound to HEATR2 antibodies, and airway cells transduced with a HEATR2-EGFP fusion protein, suggested that HEATR2, SPAG1, and DNAAF2 were present in the same foci (Fig. 2*B* and Fig. S4*A*). The interaction between these three proteins was further tested by performing immunoprecipitation studies using anti-GFP antibodies in hTECs transduced with HEATR2-EGFP or EGFP. Immunoprecipitations performed in cells obtained during the stage of active cilia growth (ALI day 12) detected SPAG1 and DNAAF2 in cells transduced by HEATR2-EGFP, but not EGFP alone (Fig. 2*C* and Fig. S4 *B*–*E*), supporting their interaction and suggesting specific localized clusters of proteins for preassembly.

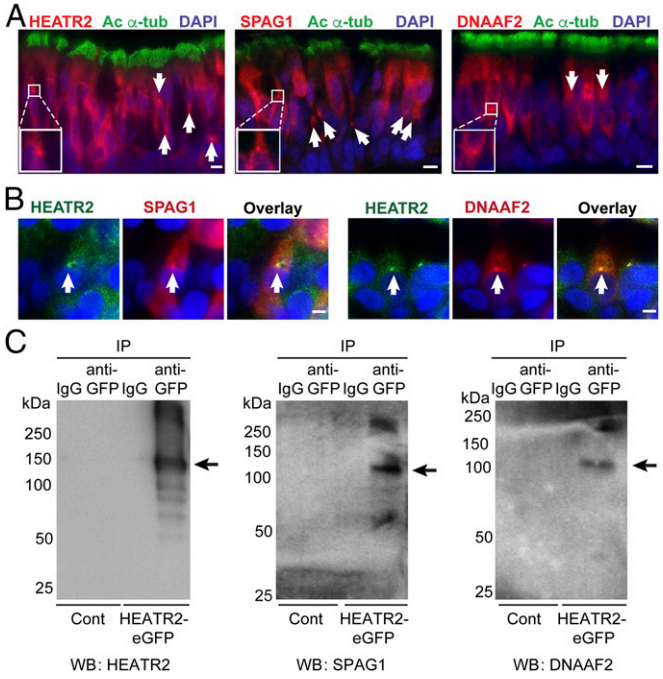

Fig. 2. HEATR2 colocalizes with and binds SPAG1 and DNAAF2. (*A*) Normal human tracheal tissue immunostained for HEATR2, DNAAF2, or SPAG1 (all red) and acetylated α-tubulin (green). (*Insets*) Prominent perinuclear foci. Arrows indicate additional foci. (*B*) Normal human nasal epithelial cells cultured using ALI conditions immunostained for early preassembly proteins. SPAG1 and DNAAF2 were detected using fluorescently labeled secondary antibodies (red), and HEATR2 was detected using anti-HEATR2 antibodies labeled with fluorescent-labeled F(ab) (green). Arrows point to foci. (*C*) Immunoprecipitation of HEATR2-EGFP with SPAG1 and DNAAF2. Cultured tracheobronchial epithelial cells transduced by lentivirus with EGFP or HEATR2-EGFP were immunoprecipitated with EGFP antibody and analyzed by immunoblotting for HEATR2, SPAG1, and DNAAF2 (arrows). Nuclei were stained with DAPI (blue). WB, Western blot. (Scale bars: *A* and *B*, 10 μM.)

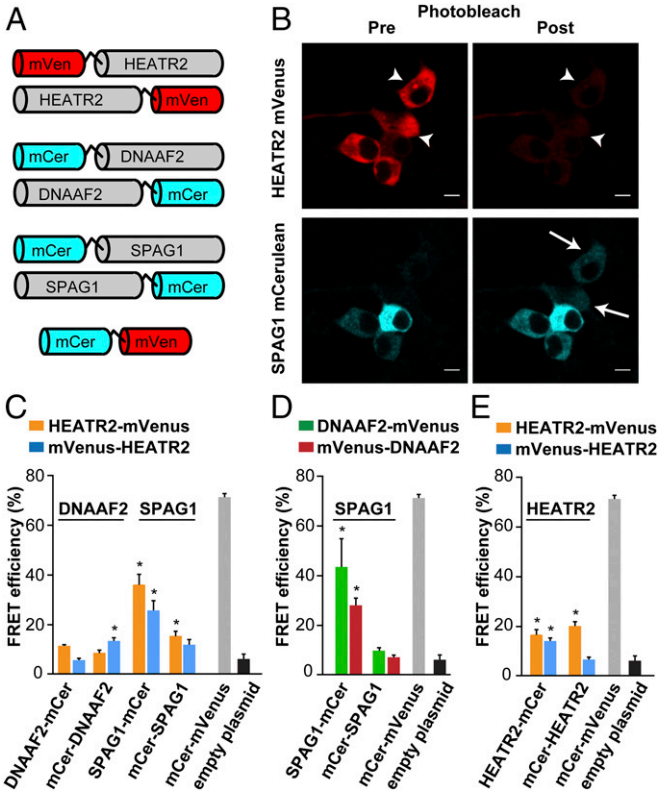

Fig. 3. FRET analysis of HEATR2 interaction with early preassembly factors. (*A*) Plasmids that express HEATR2, SPAG1, and DNAAF2 fused with the indicated fluorescent mVenus (mVen) or mCerulean (mCer) protein at the N or C terminus. Plasmids were transfected into HEK293T cells for FRET analysis. A mVen-mCer containing plasmid was the positive control, and empty plasmid was the negative control. (*B*) Representative photomicrographs of FRET images showing acceptor photobleaching (arrowheads) and increased fluorescence of the donor fluorophore (arrows). (Scale bars: 10 μM.) (*C*) FRET analysis of cells cotransfected with HEATR2 and SPAG1 plasmids compared with HEATR2 and DNAAF2 plasmids. (*D*) FRET analysis of cells cotransfected with SPAG1 and DNAAF plasmids. (*E*) FRET analysis of cells showing the interaction of HEATR2 tagged at indicated termini and fluorescent protein. Data in *C*–*E* are the mean ± SEM of $n = 3$ independent experiments. A significance difference (*$P < 0.05$) between the tested plasmids and the negative control was determined using a two-tailed Student's *t* test.

To better characterize protein–protein interactions, we performed Förster resonance energy transfer (FRET) experiments in live cells transduced with tagged preassembly proteins. HEATR2, DNAAF2, and SPAG1 were fused to either a yellow (mVenus) or blue (mCerulean) fluorescent protein (41, 42). The tags were placed at the N or C terminus of the protein (Fig. 3*A*). A dual-reporter plasmid composed of fused mVenus and mCerulean proteins separated by an eight-amino acid flexible linker (43, 44) served as a positive control, and plasmids expressing the mVenus or mCerulean fluorescent tag without a target protein served as negative controls. FRET occurs when two proteins are less than 10 nm apart. FRET was identified between HEATR2 and SPAG1 by acceptor photobleaching, resulting in dequenching and a consequent increase in donor florescence (mCerulean) (Fig. 3*B*). FRET signal analysis suggested that HEATR2 interacted directly with SPAG1 as determined by increased FRET activity between tagged HEATR2 and tagged SPAG1, compared with control plasmids (Fig. 3*C*).

The result did not change when fluorescent tags were on the N or C terminus of either protein. FRET was not detected between HEATR2 and DNAAF2; however, FRET analysis of cells transduced with DNAAF2 and SPAG1 suggested that this pair interacts directly with one other (Fig. 3*D*). We also analyzed the HEATR2–HEATR2 interactions since this is a common feature of other HEAT-repeat proteins (45). HEATR2 interacted with itself, as demonstrated by the increased FRET signal between HEATR2 pairs tagged with both mVenus and mCerulean (Fig. 3*E*). We interpret these data to mean that HEATR2 and SPAG1 are in close proximity in the cytoplasm, possibly in a complex, whereas HEATR2 interacts indirectly with DNAAF2, mediated through a complex with SPAG1.

HEAT-Repeat Domains Are Redundant for HEATR2–SPAG1 Interaction. Structure analysis based on crystallography indicates that HEAT domains stack together to form flexible scaffolds to mediate protein–protein interactions for the binding and assembly of multiple substrates (27, 28, 46). Analysis of the predicted structure of HEATR2, using Phyre2 (47), showed a structure dominated by HEAT domains and an overall concave shape that is typical of HEAT-repeat proteins (26) (Fig. 4*A*). HEAT domains contain a loosely conserved pattern of alternating hydrophilic and hydrophobic residues within the structure of antiparallel helices (48). This pattern and consensus sequence within the A- and B-helixes were identified in the 10 predicted HEAT domains of HEATR2 listed by UniProt (49) (Fig. 4*B*). To determine if a specific single HEAT domain or region of the protein is required for SPAG1 interaction, we performed N-terminus and C-terminus deletions in HEATR2 and analyzed FRET efficiency (Fig. 4 *C* and *D*). Deletions of the N terminus of HEATR2, which included HEAT domains 1–4, did not affect FRET with SPAG1. Likewise, deletions of the C terminus of HEATR2, which encompassed HEAT domains 7–10 did not abolish FRET activity. A reduction in FRET between HEATR2 and SPAG1 was observed when a short segment at the N terminus was deleted (HEAT domains 1–3). This is likely the result of a change in protein conformation and increased distance between the fluorescent probes, as the FRET level was restored when a larger segment was deleted (heat domains 1–4). Together, these results indicated that HEATR2-SPAG1 binding is not mediated by a single binding site on either the extreme N terminus or C terminus (domains 1–4 or domains 7–10), and suggest that multiple HEATR2 regions are capable of mediating an interaction with SPAG1, consistent with predicted interaction of cargoes within a broad region of the concave surface of HEAT-repeat proteins CRM1 and PP2A (50, 51).

HEATR2–SPAG1 Interaction Is Maintained in PCD Mutations. We next considered that mutations in HEATR2 causative of PCD with absent IDAs and ODAs in the cilia axoneme may interrupt HEATR2–SPAG1 interactions. We initially reported on a missense P795L mutation located within HEAT domain 10 in a patient with classic PCD features (14). Another group later reported a different mutation, similarly within HEAT domain 10 (52). We have since identified two additional mutations in HEATR2 in two families (Fig. S5 and Table S2). The proband of one family has a homozygous mutation in HEATR2 c.2353–2356del AG (p.S785Cins fs*4, referred to as S785Cins) that causes a frame shift and premature termination also within HEAT domain 10. This child had typical features of PCD. A homozygous missense mutation c.1499G > T (p.C500F) was present in two siblings of another family. This mutation lies not in a HEAT domain, but within an unstructured region between HEAT domains 6 and 7. The children with the C500F mutation had less prominent PCD symptoms, despite the presence of situs inversus totalis in one of the siblings. The C500F mutation is predicted to be pathogenic; however, the residue is conserved only in higher organisms (Fig. S5*D*). Electron microscopy analysis showed reduced numbers of IDAs and

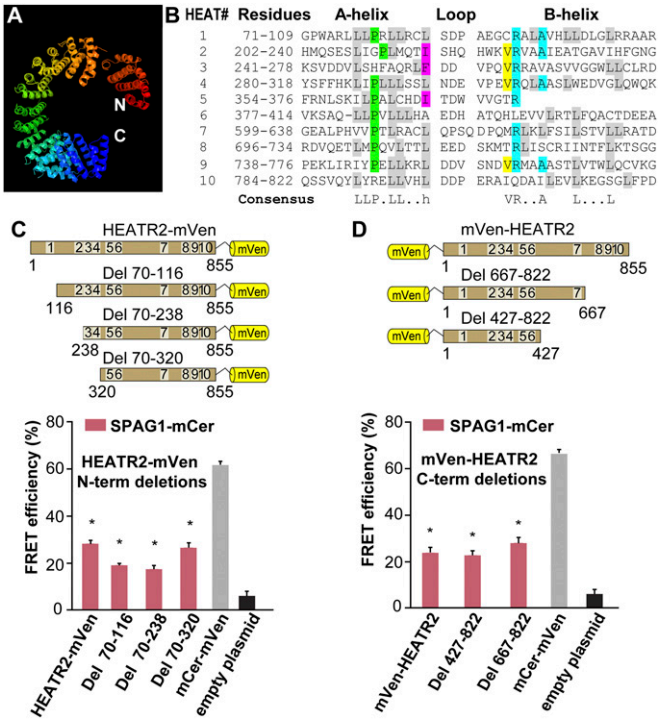

Fig. 4. HEATR2 domain interactions with SPAG1. (*A*) Predicted structure of HEATR2 showing arrangement of HEAT-repeat domains as determined by Phyre2 (47). The N and C termini are indicated. (*B*) HEAT-repeat sequences showing the predicted α- and β-helixes, the loop between helices, and the consensus sequence. Lysine residues are gray, and conserved residues in the consensus sequence are colored. Hydrophobic residues are colored magenta. (*C*) FRET analysis of HEK293T cells cotransfected with plasmids expressing the indicated HEATR2 (mVen) N-termimus (term) deletions and SPAG1 (mCer). (*D*) FRET analysis of cells cotransfected with plasmids expressing the indicated (mVen) HEATR2 C-term deletions and SPAG1 (mCer). Data in *C* and *D* are the mean ± SEM of $n = 3$ independent experiments. A significance difference (*$P < 0.05$) between the tested plasmids and the negative control was determined using a two-tailed Student's *t* test.

ODAs in all cases (Fig. S5 *A* and *B*). Cilia on cells cultured from the subject with the S785Cins mutation were immotile, as determined by high-speed video microscopy. In contrast, high-speed video analysis of cilia on cells with the C500F mutation showed variable activity, ranging from immotile to a slow beat frequency (Fig. S5*E* and Movies S1–S5).

The impact of human-specific HEATR2 mutations on SPAG1 interaction was determined using FRET. We did not observe changes in the efficiency of FRET between HEATR2 harboring patient-specific mutations and SPAG1 (Fig. 5*A*). This suggests that these HEATR2 mutations do not disrupt the direct interaction with SPAG1, and that HEAT domain 10 was dispensable for that interaction. To determine if there was a relationship between mutant HEATR2 and SPAG1 in vivo, we obtained nasal epithelial cells from children bearing HEATR2 mutations and from control, nonaffected individuals to establish ALI cultures. We observed the colocalization of HEATR2 and SPAG1 in cells from both normal control subjects and those with mutations (Fig. 5*B*). When assessing mutant cells, we did not appreciate a reduction in the number of perinuclear foci. However, we observed the accumulation of large dual-positive HEATR2-SPAG1 aggregates only in cells from subjects with PCD (Fig. 5*B*). Large aggregates were also present in HEK293T cells cotransfected with mutant HEATR2 and normal SPAG1 expression plasmids (Fig. S6*A*).

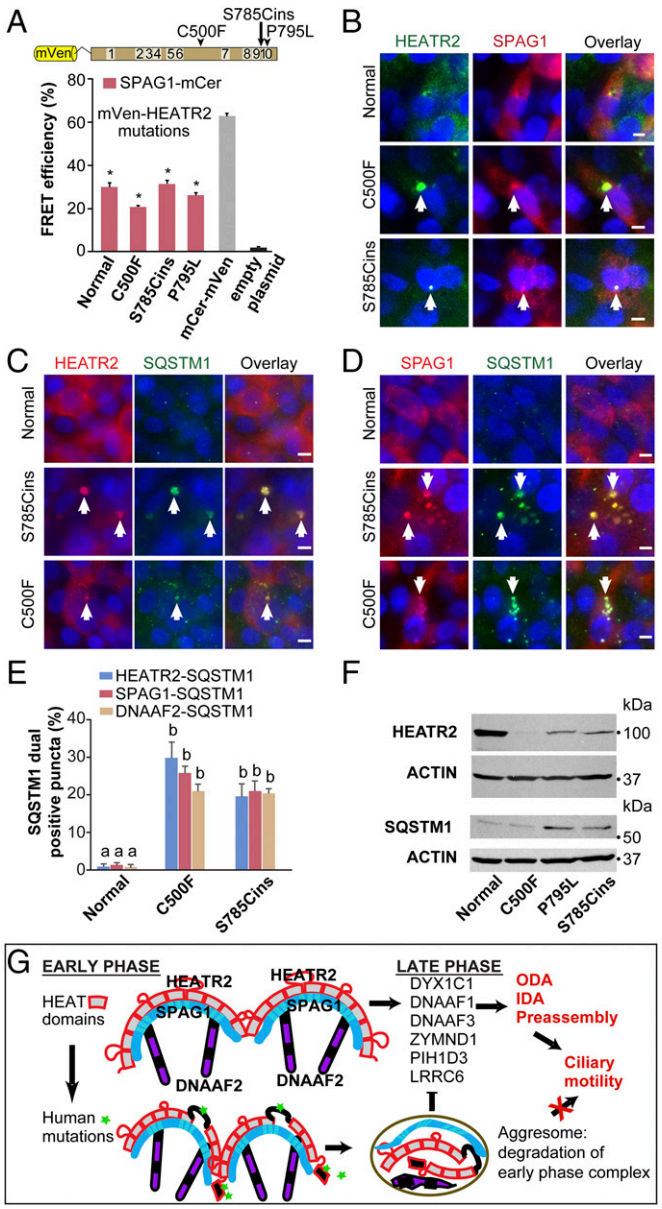

Fig. 5. HEATR2 mutations induce aggregates of preassembly proteins. (*A*) FRET analysis between SPAG1 and mutant HEATR2. Locations of mutations are shown on the cartoon of HEATR2. HEK293T cells were cotransfected with expression plasmids expressing mutant HEATR2 and normal SPAG1. FRET signal was compared with a mVen-mCer–containing plasmid and an empty plasmid negative control. (*B*) Colocalization of SPAG1 with mutant HEATR2. Primary nasal epithelial cells obtained from subjects with the indicated HEATR2 mutation were cultured at ALI and then immunostained for HEATR2 (green) and SPAG1 (red). (*C* and *D*) SQSTM1 in aggregates of cell cultures of mutant HEATR2 patient nasal cells colocalized with HEATR2 and SPAG1 by immunostaining. (*E*) Quantification of SQSTM1 puncta that are dual-positive for HEATR2, SPAG1, or DNAAF2, respectively, in normal or mutant primary nasal epithelial cells. (*F*) Immunoblot analysis showing decreased levels of HEATR2 protein and increased levels of SQSTM1 expression in nasal cells from subjects with HEATR2 mutations. (*G*) Model of interaction of early cilia preassembly proteins. In the early phase of preassembly, HEAT domains of HEATR2 multimerize and form a scaffold. HEATR2 binds SPAG1, which binds DNAAF2. In the late phase, proteins interact in a yet undetermined manner to prepare dynein proteins for transport to the cilia. Mutations in HEATR2 (stars) result in failure of scaffold formation, leading to protein degradation and formation of SQSTM1-expressing aggresomes containing members of the early preassembly complex, which undergo degradation. Nuclei were stained with DAPI (blue). (Scale bars: *B–D*, 10 μM.) Data in *A* are the mean ± SEM of $n = 3$ experiments. A significance difference (*) between the tested plasmids and the negative control was determined using a two-tailed Student's *t* test ($P < 0.05$). Data in *E* are the mean ± SEM of at least five images (151–403 cells per sample) from two different samples with each mutation. Letters in E (a vs. b) indicate means are statistically different by one-way ANOVA with Tukey multiple comparison tests.

HEATR2 Mutations Result in Degradation of an Early Preassembly Complex. Based on the larger size and atypical distribution of puncta expressing both the mutant HEATR2 and the normal SPAG1, we considered that these complexes may be subjected to a different fate than nonmutant HEATR2. Sequestosome-1 (SQSTM1; p62) can serve as a marker for aggregates containing misfolded proteins that are subjected to cellular quality control and degradation through proteostasis (53). There were an increased number of SQSTM1/p62-positive puncta in nasal epithelial cells from subjects bearing HEATR2 mutations compared with non-PCD samples, as detected by immunofluorescent staining (Fig. 5 *C–E*). SQSTM1 also colocalized with SPAG1 and DNAAF2 in the HEATR2 mutant cells (Fig. 5*D* and Fig. S6*B*). These results suggest that in the presence of HEATR2 mutations, there is instability of the early preassembly complex. In support, we observed reduced HEATR2 protein by immunoblot analysis of primary mutant HEATR2 nasal cells (Fig. 5*F*). SPAG1 was also reduced (Fig. S6*C*). The reduction of these protein levels was accompanied by normal RNA expression (Fig. S6*D*).

To further investigate the cause of low HEATR2 protein levels, we determined the relative half-lives of the HEATR2 mutants by treating cells transfected with normal or mutant HEATR2 with cycloheximide (Fig. S7 *A* and *B*). We found that mutant forms that cause severe disease were unstable, while the C500F mutation, associated with a mild phenotype, was stable. To explore potential pathways of HEATR2 degradation, we treated CHO cells expressing mutant HEATR2 with the proteasome inhibitor MG132 (54). MG132 treatment did not increase HEATR2 protein (Fig. S7*C*), suggesting that the proteasome is not the dominant pathway for mutated HEATR2 degradation. To examine autophagy as an alternative pathway for mutant HEATR2 turnover, we treated transfected cells with chloroquine (55). As expected, chloroquine treatment increased levels of LC3BII, a marker of autophagosomes and a substrate for autophagy. However, HEATR2 proteins were not increased by chloroquine treatment, suggesting that autophagy is not the dominant mechanism for mutant HEATR2 degradation. Still, overexpression of HEATR2 mutant proteins produced a trend toward reduced autophagic activity, as indicated by the somewhat lower LC3B turnover (Fig. S7 *D* and *E*). Together, we find that the low levels of mutant HEATR2 levels are a function of their instability with degradation by a proteasome- and autophagy-independent pathway (56).

Finally, we considered that protein instability observed in HEATR2 mutation-bearing cells may be the result of defective HEATR2–HEATR2 interactions for scaffold formation. We evaluated FRET efficiency of HEATR2–HEATR2 interactions in the setting of mutations or deletions. There was no reduction in FRET between nonmutant HEATR2 and HEATR2 harboring mutations or deletions, which suggests that multimer interaction is also not dependent on a single HEAT domain (Fig. S6*E*).

In summary, our observations support a model in which early expression of HEATR2 serves as a scaffold for the establishment of an initial complex for motor protein processing in motile ciliogenesis, and that a motile ciliopathy can result from an early complex disruption (Fig. 5*G*).

Discussion

Exome sequencing has identified 10 proteins that are mutated in patients with PCD and result in the absence of the IDA and ODA multiprotein complexes in the ciliary axoneme. The current

paradigm is that these proteins, and others not yet identified, interact in a stepwise fashion to organize, fold, and transport the large dynein arm complexes (11, 15, 23). To gain a perspective on this pathway, we explored the temporal relationship of these known cilia preassembly factors, uncovering the expression of an early group and a late group in relation to FOXJ1. We found that an early group, led by HEATR2 and including SPAG1 and DNAAF2, colocalized and interacted within discrete cytoplasmic foci. We propose that the early expression of HEATR2 serves as a primary platform to establish an initial complex for motor protein processing in motile ciliogenesis. Mutation in HEATR2 results in degradation of the initial scaffold and proteostasis of the early complex that leads to disease (Fig. 5*G*).

Regulation of motile ciliogenesis occurs in two phases: an early MCIDAS-dependent portion to induce centriologenesis and later a FOXJ1 program. We found that the onset of the early preassembly program was not dependent on either factor. Conditional *MCIDAS* expression in iPSCs suggested that *HEATR2*, *DNAAF2*, and, to a lesser extent, *SPAG1* expression was independent of *MCIDAS* control. Moreover, *HEATR2* was expressed in *Foxj1*-deficient trachea. A comprehensive report of *TP73*, another factor that regulates ciliogenesis, did not identify direct regulation of preassembly genes (34). In addition, the preassembly pathway is initiated before the appearance of deuterosome generation, which is regulated by MCIDAS and has classically been considered the first mark of ciliogenesis in multiciliated cells. We interpret these findings to suggest either that there are yet undefined ciliogenesis regulatory factors or that HEATR2 and other early preassembly proteins are regulated by a program independent of ciliogenesis and parallel to centriologenesis. Support for the latter concept is the widespread expression of HEATR2, SPAG1, and DNAAF2 in nonmotile tissues as cataloged in ProteomicsBD (57).

Our data show that early-phase preassembly proteins are expressed in a characteristic pattern of cytoplasmic puncta, with additional perinuclear foci. We had previously reported that cytoplasmic HEATR2 does not colocalize with the endoplasmic reticulum, lysosomes, or basal bodies (14). We now show a similar pattern for SPAG1, and DNAAF2, which colocalize with HEATR2, using a combination of antibodies and GFP-labeled HEATR2-transduced human airway epithelial cells. The early complex forms well before the expression of dynein arm proteins. However, we also observe colocalization of DNAI1 just before the emergence of cilia, suggesting that the early complex machinery may have a role in the late phase, within the same huge multiprotein clusters. Antibody availability has limited the characterization and localization of preassembly proteins and their isoforms. Dissecting the contents of the foci relative to different protein isoforms and posttranslational modification will be important for elucidating the preassembly pathway.

HEAT-repeat proteins are ideal candidates for binding SPAG1 to HEATR2 and for providing an initial scaffold for a larger preassembly complex. HEAT–HEAT domain interactions result in stacks of repeat sequences that provide concave surfaces, which are flexible to hold large complexes within a HEATR2 pocket (26). Our FRET studies demonstrate that HEATR2 interacts with itself, possibly forming dimers or multimers as observed with other HEAT-repeat proteins (58, 59), which is ideal for binding large numbers of ligands, for example, several SPAG1 molecules. SPAG1 sites for interactions with HEATR2 are not yet identified. SPAG1 contains multiple tetratricopeptide repeat domains that may mediate protein–protein interaction and assembly of multiprotein complexes (60).

Given the enrichment of mutations in HEAT domain 10, it seems possible that this was a key site for HEATR2–SPAG1 interactions. However, this was not the case, and, in fact, deletions of the C and N termini did not alter FRET between HEATR2 and SPAG1, suggesting that these regions alone are not essential to maintain this interaction, and that HEATR2–SPAG1 interactions may occur at multiple locations. We also identified a mutation outside a HEAT-repeat domain causative of PCD. Disruption of the lengthy sequence of residues between HEAT domains 6 and 7 possibly affects early complex formation by interrupting the stacking of these two central HEAT domains.

HEATR2 mutations resulted in the appearance of large SQSTM1-positive aggregates within both primary cells and cell lines expressing mutant HEATR2. These aggregates also contained SPAG1 and DNAAF2, suggesting the formation and degradation of a larger HEATR2–SPAG1–DNAAF2 complex, rather than only HEATR2. Turnover of mutated HEATR2 does not appear to be a substrate of the protostome or autophagy. While these pathways constitute the major routes for degradation, other pathways exist and could be contributing to the early preassembly complex degradation (56). Stabilizing the mutant preassembly complex, which our data suggest is still capable of binding SPAG1, could potentially provide future therapy for subjects with PCD.

In addition to placing HEATR2 in an early, central position of preassembly, we can now better position DNAAF2 in an early pathway. While we found that SPAG1 binds DNAAF2, others have reported that the late preassembly proteins DYX1C1 and PIH1D3 also bind DNAAF2 (16, 20). Thus, we postulate that DNAAF2 can function as a link between the early- and late-phase complexes. DNAAF2 and other preassembly proteins may be guided into specific positions between early and late phase by the chaperone function of heat shock proteins (61). HSP70 has been shown to bind DNAAF2 (11), and HSP90 binds DYX1C1 (16, 62). How any of these proteins interact with a preassembly complex or dynein proteins and participate in the organization of the IDA and ODA is an important goal for future studies and potential therapeutic manipulation.

Based on our data and those of others (11, 15, 21, 61), we propose a model of early motile cilia preassembly (Fig. 5*G*). We postulate that HEATR2 multimers form a flexible scaffold that binds several SPAG1 molecules, which, in turn, bind multiple DNAAF2 molecules. These interactions might be transient in nature, changing as cell differentiation progresses and FOXJ1 is activated. For example, DNAAF2 might be released from SPAG1 for binding with PIH1D3 and DYX1C1 for folding of dynein motor proteins into the IDA and ODA (21). The stoichiometry of the early preassembly protein complex interaction must be determined, but the ability of HEATR2 to multimerize into a docking platform that binds many molecules of SPAG1 and DNAAF2 would provide a mechanism for amplification for rapid preassembly, which would allow the simultaneous fabrication of thousands of motor units for delivery to hundreds of axoneme microtubules during ciliogenesis.

Methods

Human Subjects. Protocols were approved by the Institutional Review Board at Washington University in St. Louis. Patients were evaluated at the rare airway disease and PCD clinic at St. Louis Children's Hospital at Washington University. Informed consent was obtained from individuals (or their legal guardians). Nasal epithelial cells were obtained from the inferior turbinate for transmission electron microscopy or culture as previously described (14).

Airway Epithelial Cells. Human airway epithelial cells were isolated from surgical excess of tracheobronchial segments of lungs donated for transplantation as previously described and were exempt from regulation by US Department of Health and Human Services regulation 45 Code of Federal Regulations Part 46 (14). Tracheobronchial and nasal epithelial cells were expanded in culture, seeded on supported membranes (Transwell; Corning, Inc.), and differentiated using ALI conditions (14, 31), as detailed in *Supporting Information*.

iPSCs. The iPSCs were generated from wild-type human foreskin fibroblasts using a cre-recombinase excisable polycistronic lentivirus as described previously (36). Differentiation was carried out as previously described

followed by culture using ALI conditions (36), as detailed in *Supporting Information*.

Mouse Trachea. All animal studies were approved by the Institutional Animal Care and Use Committee at Washington University in St. Louis. Trachea samples were obtained from wild-type and *Foxj1* null mice (37).

RT-PCR Analyses. RNA expression was assessed by RT-PCR amplification using gene-specific primers (Table S3) with SYBR green nucleic acid labeling as described in *Supporting Information*.

Epithelial Cell Immunofluorescent Staining and Immunoblot Analyses. Airway cells were fixed and immunostained as previously described using antibodies listed in Table S4 (31, 63). Nuclei were stained using DAPI (Vector Laboratories). F(ab) fragment labeling of primary antibodies was performed following the manufacturer's instructions (Zenon; Invitrogen). Images were acquired using an epifluorescent microscope interfaced with imaging software (LAS X; Leica) and adjusted globally for brightness and contrast using Photoshop (Adobe Systems).

Expression Plasmids. Plasmids containing sequences of HEATR2, SPAG1, and DNAAF1 for transfection and FRET studies were generated as described in *Supporting Information*.

High-Speed Video Microscopy. Cilia beat frequency was analyzed live in at least five fields obtained from each preparation using a high-speed video camera and was processed with the Sisson-Ammons Video Analysis system (Ammons Engineering) as described (14, 64).

Immunoblot Analysis. Protein extraction from tissue or cells and immunoblot analysis were performed as previously described (63), using antibodies listed in Table S4.

Immunoprecipitation. Human airway epithelial cells were transduced with EGFP or HEATR2-EGFP using recombinant lentivirus, differentiated using ALI conditions as previously described (32), and then prepared for HEATR2 immunoprecipitation with GFP antibodies (Table S4). Details are provided in *Supporting Information*.

FRET Imaging. Images to measure FRET efficiency were acquired on a confocal microscopy system equipped with a spectral detector of laser-activated fluorescence (LSM 880; Karl Zeiss). Percent FRET efficiency (E) was calculated by measuring the donor fluorescence intensity (I_D) before and after the acceptor photobleaching $E = 100 * (I_{D\text{-}after} - I_{D\text{-}before})/I_{D\text{-}after}$. Cells with an acceptor/donor intensity ratio outside of the 1:8–8:1 range were excluded from the analysis to avoid artifacts. Additional details are provided in *Supporting Information*.

Assessment of Protein Degradation. Assays were performed in CHO cells that were transfected with normal or HEATR2 mutants for 24 h before treatment. To determine protein stability, cells were treated with cycloheximide (200 μg/mL) 24 h posttransfection and then analyzed by immunoblotting for HEATR2 expression up to 24 h later. In other experiments, transduced cells were treated with MG132 (10 μM) for 4 h and then evaluated for HEATR2 expression by immunoblotting. Autophagy activity was determined using the LC3B turnover assay (65, 66). Cells were treated with chloroquine (50 μM) for 2 h, and LC3BII levels were analyzed by immunoblotting as previously described (55, 65).

Statistical Analyses. Group variation is described as the mean ± SE (SEM). Statistical comparisons between groups were made using one-way ANOVA with Tukey post hoc analysis. Individual group differences were determined using a two-tailed Student's *t* test. A *P* value of 0.05 was considered to represent a significant difference. Nonparametric data are shown as the median and the 25th and 75th interquartile ranges. Data were analyzed using Prism (GraphPad). K-means cluster analysis of preassembly gene transcript levels during in vitro differentiation was performed using the K-means function, with k = 2, and the city-block distance option in MATLAB (release R2015a; MathWorks).

ACKNOWLEDGMENTS. We thank M. Davidson and S. Vogel for providing mVenus and mCerulean expression plasmids and Alan Schwartz, Brian Hackett, Alina Oltean, Susan Dutcher, Moe Mahjoub, and members of the Washington University Cilia Group for critical comments. This work was funded by awards from the American Thoracic Society Foundation/Primary Ciliary Dyskinesia Foundation/Kovler Family Foundation (to A.H.) and by NIH Grant HL128370 (to S.L.B.). FRET imaging was partially supported by a Washington University Center for Cellular Imaging award through a grant from The Children's Discovery Institute of Washington University and St. Louis Children's Hospital (Grant CDI-CORE-2015-505) and by the Foundation for Barnes-Jewish Hospital (Grant 3770). S.L.B. is the Dorothy and Hubert Moog Professor of Pulmonary Medicine, partially supported by the Foundation for Barnes-Jewish Hospital.

1. Sakato M, King SM (2004) Design and regulation of the AAA+ microtubule motor dynein. *J Struct Biol* 146:58–71.
2. Wirschell M, et al. (2009) IC97 is a novel intermediate chain of I1 dynein that interacts with tubulin and regulates interdoublet sliding. *Mol Biol Cell* 20:3044–3054.
3. VanderWaal KE, et al. (2011) bop5 mutations reveal new roles for the IC138 phosphoprotein in the regulation of flagellar motility and asymmetric waveforms. *Mol Biol Cell* 22:2862–2874.
4. Kubo T, Yagi T, Kamiya R (2012) Tubulin polyglutamylation regulates flagellar motility by controlling a specific inner-arm dynein that interacts with the dynein regulatory complex. *Cytoskeleton (Hoboken)* 69:1059–1068.
5. Pennarun G, et al. (1999) Loss-of-function mutations in a human gene related to Chlamydomonas reinhardtii dynein IC78 result in primary ciliary dyskinesia. *Am J Hum Genet* 65:1508–1519.
6. Olbrich H, et al. (2002) Mutations in DNAH5 cause primary ciliary dyskinesia and randomization of left-right asymmetry. *Nat Genet* 30:143–144.
7. Ostrowski LE, et al. (2002) A proteomic analysis of human cilia: Identification of novel components. *Mol Cell Proteomics* 1:451–465.
8. Davis SD, et al. (2015) Clinical features of childhood primary ciliary dyskinesia by genotype and ultrastructural phenotype. *Am J Respir Crit Care Med* 191:316–324.
9. Hirokawa N, Tanaka Y, Okada Y, Takeda S (2006) Nodal flow and the generation of left-right asymmetry. *Cell* 125:33–45.
10. Loges NT, et al. (2009) Deletions and point mutations of LRRC50 cause primary ciliary dyskinesia due to dynein arm defects. *Am J Hum Genet* 85:883–889.
11. Omran H, et al. (2008) Ktu/PF13 is required for cytoplasmic pre-assembly of axonemal dyneins. *Nature* 456:611–616.
12. Kott E, et al. (2012) Loss-of-function mutations in LRRC6, a gene essential for proper axonemal assembly of inner and outer dynein arms, cause primary ciliary dyskinesia. *Am J Hum Genet* 91:958–964.
13. Horani A, et al. (2013) LRRC6 mutation causes primary ciliary dyskinesia with dynein arm defects. *PLoS One* 8:e59436.
14. Horani A, et al. (2012) Whole-exome capture and sequencing identifies HEATR2 mutation as a cause of primary ciliary dyskinesia. *Am J Hum Genet* 91:685–693.
15. Mitchison HM, et al. (2012) Mutations in axonemal dynein assembly factor DNAAF3 cause primary ciliary dyskinesia. *Nat Genet* 44:381–389, S1–S2.
16. Tarkar A, et al.; UK10K (2013) DYX1C1 is required for axonemal dynein assembly and ciliary motility. *Nat Genet* 45:995–1003.
17. Knowles MR, et al. (2013) Mutations in SPAG1 cause primary ciliary dyskinesia associated with defective outer and inner dynein arms. *Am J Hum Genet* 93:711–720.
18. Zariwala MA, et al. (2013) ZMYND10 is mutated in primary ciliary dyskinesia and interacts with LRRC6. *Am J Hum Genet* 93:336–345.
19. Austin-Tse C, et al. (2013) Zebrafish ciliopathy screen plus human mutational analysis identifies C21orf59 and CCDC65 defects as causing primary ciliary dyskinesia. *Am J Hum Genet* 93:672–686.
20. Paff T, et al. (2017) Mutations in PIH1D3 cause X-linked primary ciliary dyskinesia with outer and inner dynein arm defects. *Am J Hum Genet* 100:160–168.
21. Olcese C, et al.; UK10K Rare Group (2017) X-linked primary ciliary dyskinesia due to mutations in the cytoplasmic axonemal dynein assembly factor PIH1D3. *Nat Commun* 8:14279.
22. Freshour J, Yokoyama R, Mitchell DR (2007) Chlamydomonas flagellar outer row dynein assembly protein ODA7 interacts with both outer row and I1 inner row dyneins. *J Biol Chem* 282:5404–5412.
23. Fowkes ME, Mitchell DR (1998) The role of preassembled cytoplasmic complexes in assembly of flagellar dynein subunits. *Mol Biol Cell* 9:2337–2347.
24. Piperno G, Mead K (1997) Transport of a novel complex in the cytoplasmic matrix of Chlamydomonas flagella. *Proc Natl Acad Sci USA* 94:4457–4462.
25. Fok AK, Wang H, Katayama A, Aihara MS, Allen RD (1994) 22S axonemal dynein is preassembled and functional prior to being transported to and attached on the axonemes. *Cell Motil Cytoskeleton* 29:215–224.
26. Yoshimura SH, Hirano T (2016) HEAT repeats - Versatile arrays of amphiphilic helices working in crowded environments? *J Cell Sci* 129:3963–3970.
27. Groves MR, Hanlon N, Turowski P, Hemmings BA, Barford D (1999) The structure of the protein phosphatase 2A PR65/A subunit reveals the conformation of its 15 tandemly repeated HEAT motifs. *Cell* 96:99–110.
28. Vetter IR, Arndt A, Kutay U, Görlich D, Wittinghofer A (1999) Structural view of the Ran-Importin beta interaction at 2.3 A resolution. *Cell* 97:635–646.
29. Bazan JF, Kajava AV (2015) Designs on a curve. *Nat Struct Mol Biol* 22:103–105.
30. Oda T, Yanagisawa H, Kamiya R, Kikkawa M (2014) A molecular ruler determines the repeat length in eukaryotic cilia and flagella. *Science* 346:857–860.

31. You Y, Richer EJ, Huang T, Brody SL (2002) Growth and differentiation of mouse tracheal epithelial cells: Selection of a proliferative population. *Am J Physiol Lung Cell Mol Physiol* 283:L1315–L1321.
32. Horani A, Nath A, Wasserman MG, Huang T, Brody SL (2013) Rho-associated protein kinase inhibition enhances airway epithelial basal-cell proliferation and lentivirus transduction. *Am J Respir Cell Mol Biol* 49:341–347.
33. You Y, et al. (2004) Role of f-box factor foxj1 in differentiation of ciliated airway epithelial cells. *Am J Physiol Lung Cell Mol Physiol* 286:L650–L657.
34. Marshall CB, et al. (2016) p73 is required for multiciliogenesis and regulates the Foxj1-associated gene network. *Cell Rep* 14:2289–2300.
35. Quigley IK, Kintner C (2017) Rfx2 stabilizes Foxj1 binding at chromatin loops to enable multiciliated cell gene expression. *PLoS Genet* 13:e1006538.
36. Firth AL, et al. (2014) Generation of multiciliated cells in functional airway epithelia from human induced pluripotent stem cells. *Proc Natl Acad Sci USA* 111:E1723–E1730.
37. Brody SL, Yan XH, Wuerffel MK, Song SK, Shapiro SD (2000) Ciliogenesis and left-right axis defects in forkhead factor HFH-4-null mice. *Am J Respir Cell Mol Biol* 23:45–51.
38. Neesse A, et al. (2007) Sperm-associated antigen 1 is expressed early in pancreatic tumorigenesis and promotes motility of cancer cells. *Oncogene* 26:1533–1545.
39. Yu X, Ng CP, Habacher H, Roy S (2008) Foxj1 transcription factors are master regulators of the motile ciliogenic program. *Nat Genet* 40:1445–1453.
40. Vladar EK, Stearns T (2007) Molecular characterization of centriole assembly in ciliated epithelial cells. *J Cell Biol* 178:31–42.
41. Piston DW, Kremers GJ (2007) Fluorescent protein FRET: The good, the bad and the ugly. *Trends Biochem Sci* 32:407–414.
42. Piston DW, Rizzo MA (2008) FRET by fluorescence polarization microscopy. *Methods Cell Biol* 85:415–430.
43. Reddy Chichili VP, Kumar V, Sivaraman J (2013) Linkers in the structural biology of protein-protein interactions. *Protein Sci* 22:153–167.
44. Evers TH, van Dongen EM, Faesen AC, Meijer EW, Merkx M (2006) Quantitative understanding of the energy transfer between fluorescent proteins connected via flexible peptide linkers. *Biochemistry* 45:13183–13192.
45. Chook YM, Blobel G (1999) Structure of the nuclear transport complex karyopherin-beta2-Ran x GppNHp. *Nature* 399:230–237.
46. Enenkel C, Schülke N, Blobel G (1996) Expression in yeast of binding regions of karyopherins alpha and beta inhibits nuclear import and cell growth. *Proc Natl Acad Sci USA* 93:12986–12991.
47. Kelley LA, Mezulis S, Yates CM, Wass MN, Sternberg MJ (2015) The Phyre2 web portal for protein modeling, prediction and analysis. *Nat Protoc* 10:845–858.
48. Kobe B, et al. (1999) Turn up the HEAT. *Structure* 7:R91–R97.
49. Pundir S, Martin MJ, O'Donovan C (2017) UniProt protein knowledgebase. *Methods Mol Biol* 1558:41–55.
50. Monecke T, Dickmanns A, Ficner R (2014) Allosteric control of the exportin CRM1 unraveled by crystal structure analysis. *FEBS J* 281:4179–4194.
51. Tsytlonok M, et al. (2013) Complex energy landscape of a giant repeat protein. *Structure* 21:1954–1965.
52. Diggle CP, et al. (2014) HEATR2 plays a conserved role in assembly of the ciliary motile apparatus. *PLoS Genet* 10:e1004577.
53. Cha-Molstad H, et al. (2017) p62/SQSTM1/Sequestosome-1 is an N-recognin of the N-end rule pathway which modulates autophagosome biogenesis. *Nat Commun* 8:102.
54. Goldberg AL (2012) Development of proteasome inhibitors as research tools and cancer drugs. *J Cell Biol* 199:583–588.
55. Dickinson JD, et al. (2016) IL13 activates autophagy to regulate secretion in airway epithelial cells. *Autophagy* 12:397–409.
56. Taggart C, et al. (2017) Protean proteases: At the cutting edge of lung diseases. *Eur Respir J* 49:1501200.
57. Wilhelm M, et al. (2014) Mass-spectrometry-based draft of the human proteome. *Nature* 509:582–587.
58. Sawicka M, et al. (2016) The dimeric architecture of checkpoint kinases Mec1ATR and Tel1ATM reveal a common structural organization. *J Biol Chem* 291:13436–13447.
59. Lau WC, et al. (2016) Structure of the human dimeric ATM kinase. *Cell Cycle* 15: 1117–1124.
60. Blatch GL, Lässle M (1999) The tetratricopeptide repeat: A structural motif mediating protein-protein interactions. *BioEssays* 21:932–939.
61. Pal M, et al. (2014) Structural basis for phosphorylation-dependent recruitment of Tel2 to Hsp90 by Pih1. *Structure* 22:805–818.
62. Chen Y, et al. (2009) A novel role for DYX1C1, a chaperone protein for both Hsp70 and Hsp90, in breast cancer. *J Cancer Res Clin Oncol* 135:1265–1276.
63. Pan J, You Y, Huang T, Brody SL (2007) RhoA-mediated apical actin enrichment is required for ciliogenesis and promoted by Foxj1. *J Cell Sci* 120:1868–1876.
64. Sisson JH, Stoner JA, Ammons BA, Wyatt TA (2003) All-digital image capture and whole-field analysis of ciliary beat frequency. *J Microsc* 211:103–111.
65. Klionsky DJ, et al. (2012) Guidelines for the use and interpretation of assays for monitoring autophagy. *Autophagy* 8:445–544.
66. Haspel J, et al. (2011) Characterization of macroautophagic flux in vivo using a leupeptin-based assay. *Autophagy* 7:629–642.